Fluctuations of particles inside flat-bottomed funnel flow silo

Dancheng Zhang[a,b] ,Xiaodong Yang[a,b], Jinhui Zhan[a], Xiaoxing Liu[a,b,*]

[a] State Key Laboratory of Multiphase Complex Systems, Institute of Process Engineering,

Chinese Academy of Science, Beijing 100190, China

[b] School of Chemical Engineering, University of Chinese Academy of Sciences, Beijing 100049, China

Abstract

In this work the flow behavior of granular material in flat-bottomed funnel flow silos was investigated through 3D Discrete Element Method (DEM) simulations. It is observed that particles in the main part of flowing zone move collectively, manifested by the oscillatory fluctuations of the spatially averaged particle vertical velocity and the non-Gaussian characteristics of the fluctuations of individual velocity around the average. The delayed correlations of velocity fluctuations at different vertical positions and the Fourier spectrums of vertical velocity and contact force between particles were analyzed to characterize the propagation of flow fluctuation. It is found that there exist two special vertical positions in the converging part of the flowing zone. The lower one corresponds to the emission source from which the velocity wave propagates both upwards and downwards. The higher one locates at the upper boundary of converging part of the flowing zone and is characterized by the most violent fluctuation of contact force. Possible mechanisms of the appearances of these two vertical positions are discussed.

Keywords: Granular flow; Fluctuation; Wave; Silo; Discrete Element Method (DEM)

1. Introduction

Silos are commonly used in various industrial processes for the storage, handling and transportation of granular assemblies. During discharge, granular materials in silo can present complicated flow behavior. Depending on the structure of silo, particle properties, and initial packing height, the granular material in silo could be in uniform flow (mass flow) or flow surrounded by stagnant zones (funnel flow) [1]. For a flat-bottomed silo, stagnant zones will inevitably appear in the bottom corners and thus the bulk solids could be either in semi-mass flow or funnel flow. Therefore, there might coexist three distinct regimes in silo: rapid flow regime (the free fall zone right above the outlet), quasi-static regime (the stagnant zone) and the intermediate dense flow regime (plug flow zone/the upper part of funnel flow zone). The rheology of granular material, especially the rheological behavior across different regimes, has aroused great interests in the physical research field [2,3]. Thus, granular flow in silo has attracted greatest interests from the communities of both fundamental and engineering sciences.

One peculiar aspect of silo discharge frequently reported in literature is the observation of the self-excited dynamic effect in the form of strong vibrations or pulsation [4-6]. This phenomenon manifests itself in the violent fluctuations of local stress in the stress field and the sudden acceleration and subsequent deceleration of particle movement in velocity field. Experimental and numerical results demonstrate that the fluctuations of stress and particle velocity are strongly correlated and the former precedes the latter, suggesting velocity fluctuation is a direct result of the dynamic variation of stress [7-9]. For mass/semi-mass flow

silo, this self-excited dynamic effect could lead to instantaneous stress far larger than the average one, which might subsequently cause the serious fatigue or even catastrophic collapse of the silo [6]. Thus, this phenomenon has been extensively investigated both experimentally and numerically for mass/semi-mass flow silos and different sources of this dynamic excitation have been proposed [4,6,10]. Typical explanations of the physical mechanisms include the stick-slip behavior between the bulk solids and the silo walls, alternating flow patterns during flow, and the intermittent collapse of free-fall arches right above the outlet. The stick-slip mechanism is based on the observation of the formation of shear zone in the vicinity of silo wall and argues that the intense shear in this thin zone is the source of the violent fluctuation of stress [4,5,10]. In silos, the flowing zone starts to converge downwardly at the so-called Effective Transition Point (ETP). Because of the converging cross-section of the flowing zone, shear zones emanating from the silo wall might be created at ETP, expand towards the interior of bulk solids, and move downwards [6]. The alternating flow pattern mechanism states that the intermittent formation of shear zone at ETP is the direct source of the strong fluctuations of wall stress and particle velocity [11-13]. The free-fall arch mechanism assumes that right above the outlet there exists a region in which force chain network appears intermittently. The buildup and collapse of force chains lead to the violent fluctuations of stress in this zone, and the propagation of stress wave subsequently induces the synchronized variations of particle velocity [7,9]. Note that self-excited dynamic phenomena in silo might be due to many different mechanisms [6]. Because of the complexity of granular flow in silo, the phenomena are still not completely understood yet.

Strong fluctuations in velocity/stress field have also been observed in funnel flow silo. Baxter et al.[14] might be the first of investigating this phenomenon experimentally. These authors observed the formation and propagation of density waves in the central flowing zone during the discharge. Similar phenomena were later also reported by Le Pennec et al. [15] and Fullard et al [16]. All these researchers ascribed the appearances of fluctuations to the buildup and collapse of dynamic arches in the flowing zone. This inference is directly supported by the observation of curved arches appearing in their experiments. Nevertheless, it is not clear whether the formation of these arches was due to the internal frictional interactions between particles or simply a boundary wall effect, since in all these experiments the adopted silos were rather thin and the influences of the front and rear walls were clearly not negligible. Pulsating flow in fully three-dimensional funnel flow silo with wedged bottom has also been reported. The mechanical instability of the inclined stagnant zones is generally considered as the underlying mechanism [6,17]: due to the fluctuation of the lateral supports from the flowing zone and also the action of gravity, the inclined stationary materials might lose its mechanical stability and slip momentarily, causing the stress in the flowing zone to increase as a result of squeezing action. According to this heuristic theory, for funnel flow silo there should exit a critical inclination angle of the bottom walls for the occurrence of vibration/pulsation [17].

For funnel flow silo, the flowing zone width first increases with vertical position and then keeps nearly constant [21-23]. Experimentally, it has been found that granular materials in the up part of the flowing zone could be in plug flow state and notable velocity gradient only

appears in the narrow shear region in between the flowing and stagnant zones [16,24-28]. Thus, if we consider the interface between flowing and stagnant zones as a rough surface, the flowing pattern in funnel flow silo is actually the same as that in mass/semi-mass flow silo. It is then natural to ask whether the rheological behaviors of the flowing granular materials in these two systems are similar or not. Do strong and regular fluctuations in velocity/stress field also appear in fully three-dimensional funnel flow silo with flat bottom where the above-mentioned slipping mechanism for wedged-shape silo does not apply? Do the alternating flow pattern mechanism or free-fall arch mechanism commonly proposed to explain the dynamic excitation in mass/semi-mass flow silo also apply for funnel flow silo? In this work, we will try to answer these questions. Another reason triggering this research work is the hypothesis that the discharge of granular materials from silo seems to be controlled by the flow behavior of materials in the vicinity of outlet. It has been found both experimentally and numerically that the presence of obstacle at a proper position of the bottom converging zone can lead to higher flow rate than the case without obstacle [18-20]. Explanations to this counterintuitive phenomenon are generally based on contact dynamics. But it is also possible that the presence of obstacle changes the fluctuating characteristics of particle velocity. Thus, investigating whether regular fluctuation of particle velocity appears in funnel flow silo, and if it does, the possible underlying mechanisms, is obviously useful for better understanding of the complex flow behavior of granular materials in silos.

2. Simulation details

The simulations discussed in this work were conducted using the commercial DEM software

EDEM 2.7. The default Hertz-Mindlin contact model available in EDEM 2.7 was adopted to solve the interaction between particles and that between the particle and the wall:

$$F_n = \frac{4}{3}E^*\sqrt{R^*}\delta_n^{3/2} + 2\sqrt{\frac{5}{6}}\beta\sqrt{S_n m^*}V_n^{rel} \quad (1)$$

$$F_t = \begin{cases} S_t\delta_t + 2\sqrt{\frac{5}{6}}\beta\sqrt{S_t m^*}V_t^{rel} & |F_t| < \mu_s |F_n| \\ \mu_s F_n sign(\delta_t) & |F_t| \geq \mu_s |F_n| \end{cases} \quad (2)$$

where F_n and F_t are the components of contact force in normal and tangential directions. E^*, R^*, and m^* represent the equivalent Young's modulus, radius, and mass, and are defined as $1/E^*=(1-v_i^2)/E_i+(1-v_j^2)/E_j$, $1/R^*= 1/R_i +1/R_j$, and $1/m^*=1/m_i+1/m_j$, where E, v, R, and m is the Young's modulus, Poisson ratio, and the radius and mass of particles (i, j), respectively. $\beta=\ln e/(\ln^2 e+\pi^2)^{1/2}$, $S_n=2E^*(R^*\delta_n)^{1/2}$, $S_t= 8G^*(R^*\delta_n)^{1/2}$, G^* is effective shear modulus, δ_n and δ_t refer to normal and tangential displacements, V_n^{rel} and V_t^{rel} are normal and tangential relative translation velocities, μ_s and e are particle translational friction coefficient and restitution coefficient, respectively.

The tangential force produces an angular momentum ($I_t=RF_t$) and thus leads the particle to rotate. For real granular particles, the surface roughness and the deviation from the ideal spherical shape may limit their rotational ability. In DEM simulations, the limited rotation of particle can be accounted for by introducing a rolling resistant momentum I_r. Different rolling resistant models have been reported in literature [29-31] and the model available in EDEM 2.7 is the one proposed by Zhou et al [29],

$$I_r = \mu_r F_n R_i \boldsymbol{\omega}_i \quad (3)$$

where μ_r is the rotational friction coefficient and $\boldsymbol{\omega}_i$ is the unit angular velocity vector of particle i at the contact point. The main setting of the DEM simulation parameters is summarized in Table.1.

Table 1 Summary of simulation parameters

Type	Parameters	Value
Particle	Solids density, ρ_p (kg/m^3)	2500
	Poisson ratio, v_p	0.25
	Shear modulus, G_p (Pa)	1.5×10^8
	Diameter, d(mm)	20
Silo	Density, ρ_p (kg/m^3)	7800
	Poisson ratio, v_p	0.25
	Shear modulus, G_p (Pa)	7×10^{10}
Particle-particle	Restitution coefficient, $e_{p\text{-}p}$	0.9
	translational friction coefficient, μ_s	0.6
	rotational friction coefficient, μ_r	0.01
Particle-silo	Restitution coefficient, $e_{p\text{-}s}$	0.5
	translational friction coefficient, μ_s	0.6
	rotational friction coefficient, μ_r	0.01
Simulation	Time step, Δt(s)	1×10^{-6}

The silo considered in this work has rectangular structure with outlet located at the center of the flat bottom, as schematized in Fig.1. The lateral (y-) boundaries of the silo were modeled as flat frictional walls and the distance between them (width) was 300d (d is the average particle diameter). Periodic boundary condition was adopted in the depth (x-) direction to exclude the possible front and rear wall effects. Following our previous work [21], the depth was set as 6d. To prepare the initially packed granular assembly, gas of non-overlapping

spheres with diameter uniformly distributed between 0.95 d and 1.05 d were firstly generated in the silo domain through the particle factory module of EDEM 2.7. The sample was then densified under the action of gravity. Discharging was achieved by generating a rectangular aperture with width of W_1 (=10~40d) and depth of 6d at the central region of the flat bottom wall. To conduct continuous rather than batch discharging, a dynamic particle factory was located just above the top surface of the granular assembly and particles were continuously generated if there was generating space. The height of the granular assembly during the discharging could then be maintained as constant through this way. Unless otherwise specified, the height of the sample was kept as 300d, and the total number of particles in samples is about 700,000.

To conduct the statistical analyses, the whole silo domain was notionally mapped by grids with size of (6×6×6)d. The attainment of the steady state of discharging process was evaluated by monitoring the temporal variations of particle velocity of those grids right above the outlet (y=0). With the ongoing of discharge, the spatially averaged particle velocity magnitude first increased and then fluctuated around a constant value. All the statistical analyses were conducted after the discharging process has entered the steady state.

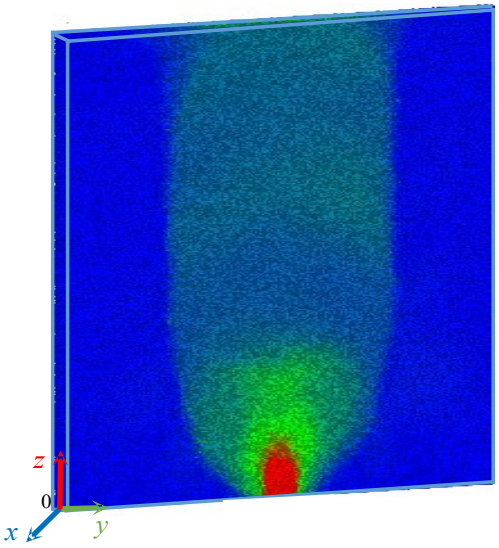

Fig.1 Schematic of the simulated flat-bottom silo

3. Results and discussion

3.1 Fluctuation of particle velocity

If without specific instruction, the simulation results presented in this sub-section was obtained from the case with W_1=20d. Within the considered value range, varying the value of W_1 did not qualitatively change the phenomena discussed below.

Fig.2a presents the horizontal distributions of temporal-spatially averaged vertical velocity at different vertical positions. It can be found that the flow mode was funnel flow. Downward movement of particles only appear in horizontal center of the silo, giving rise to the formation of stagnant zones in the vicinity of side walls. The width of the flowing zone first increases with vertical position and then levels off. Qualitatively, such phenomenon is consistent with the experimental observations reported in literature [1,22,23]. The width of the flowing zone increases with the outlet size W_1 and is weakly affected by the particle friction coefficient μ_s [32,33]. For the values of W_1 and μ_s considered in this work, it has been carefully checked

that the flow regime was always funnel flow.

Fig.2a also indicates that the shape of velocity profile changes along the upward direction. Close to the outlet, the horizontal distribution of vertical velocity component is characterized by highly peaked shape resembling a delta function, as commonly observed in granular discharge from silo. The velocity distribution curve gradually flattens along the upward direction and eventually forms a plateau in the horizontal central zone, i.e., a plug flow zone is formed in the upper part of the flowing zone. Such phenomenon has also been experimentally observed for funnel flow discharge [24-28]. Szabo et al [28] found the formation of plug flow zone was closely related to particle shape. Their experimental results show that the position of plug flow zone was closer to the outlet for longer grains. Fullard et al [10] reported that smaller outlet size led to the lower boundary of the plug flow zone. This phenomenon has also been successfully captured by our simulations, as shown in Fig.2b, where the variations of particle vertical velocity along the z- direction at y=0 for different outlet sizes are presented. It can be found that the region with constant vertical velocity monotonously shrinks with the increase of outlet size.

The experimental results of Szabo et al [28] show that particles in the plug flow zone moved synchronously and the vertical velocity field fluctuated with large amplitude. Such phenomenon has also been observed in our simulations, as demonstrated in Fig.2d. Fig.2c and d present the instantaneous vertical velocities of individual particles collected at different moments. Close to the outlet (Fig.2c), particle movement seems to be random. There is no

clear sign of spatial/temporal correlation in particle velocity. Nevertheless, in the plug flow zone (Fig.2d) aligned clouds of data points can be clearly seen, indicating the collective motion of particles in this region. The correlated movement of particles in funnel flow zone has also been reported by the group of Zuriguel [34,35]. Nevertheless, different from those presented in Fig.2a, in their experiments the temporal-spatially averaged vertical velocity profiles have a Gaussian-like shape. We conjecture that the correlated movement of particles appeared in their experiments might be ascribed to the front and rear wall effects since the depth of their silo was only around one particle diameter. As will be presented later, the collective motion of particles appeared in our simulations originates from a special zone right above and close to the outlet rather than boundary wall effect.

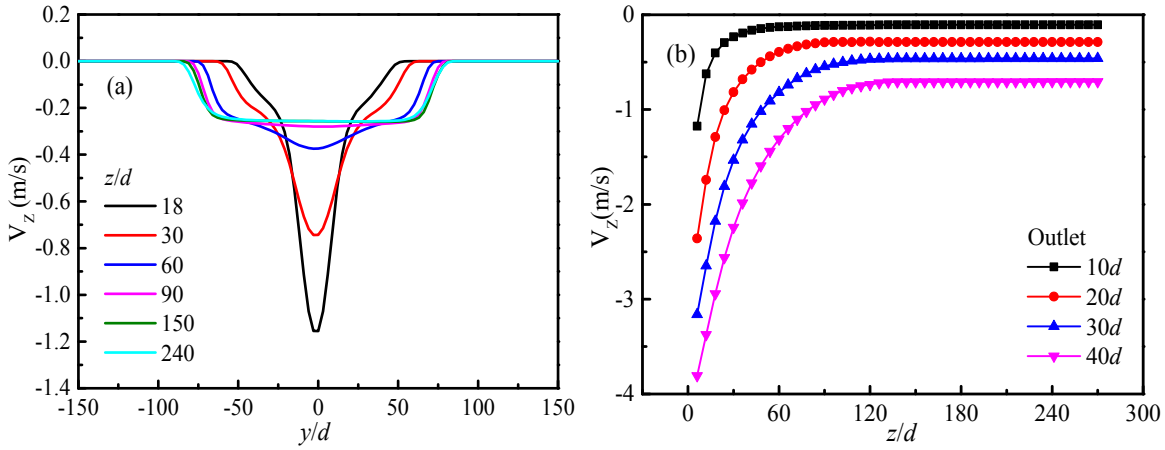

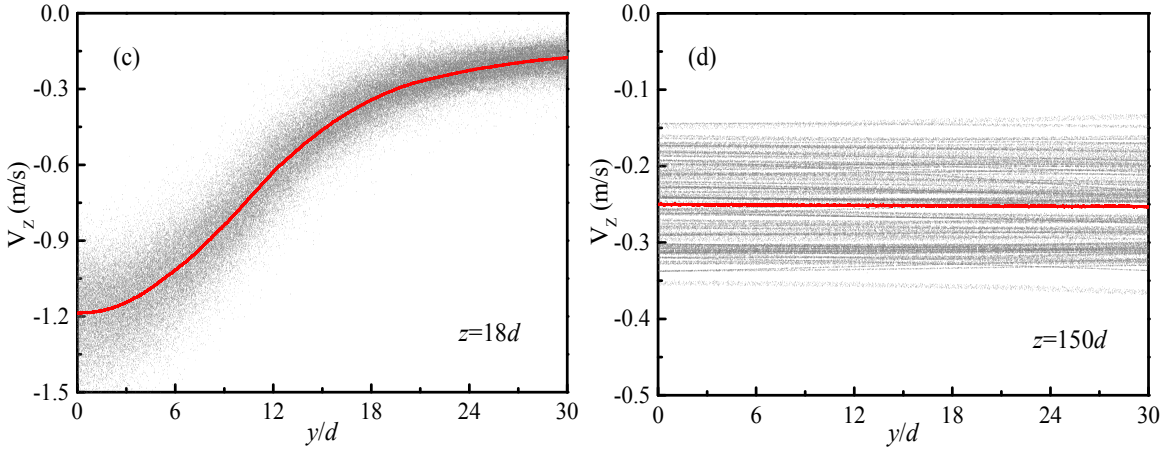

Fig.2 (a) Vertical velocity profiles at different z- positions, (b) the variations of particle vertical velocity along the z- direction at y=0 for different outlet sizes, (c) and (d) denote the instantaneous vertical velocities of individual particles collected at different moments.

To characterize the downward motion of particles, the temporal variations of spatially averaged vertical velocity at different positions have been monitored. Typical results are presented in Fig.3a. It can be found that in regions close to the outlet (z =6d) the vertical velocity varies randomly with time. This is further confirmed in Fig.3b which shows the discrete Fourier analysis results of the temporal variations of velocity shown in Fig.3a. It can be seen that at z =6d the Fourier spectrums do not present any distinguishable structure. Nevertheless, in the upper part (about z ≥60d) a well-defined periodicity of the time variation of the vertical velocity appears. In between these well-defined periodic variations there exist short time intervals in which the vertical velocity varies with less regularity. The reason for the appearance of these short time intervals is still not clear. We notice that similar phenomena have also appeared in both DEM simulations [36] and physical experiments [10], though in these works the granular assemblies were in mass flow discharge. Fig.3b indicates

that for $z \geq 60d$ the Fourier spectrums show a similar fluctuation mode with a predominant peak at the frequency of around 2.24Hz. Such results clearly suggest that in this region the flow of particles is in resonant mode. Note that in our simulations the system is in funnel flow regime. Although resonant silo discharge, also referred to as silo music, silo honking, or silo quaking, has been reported and investigated by many researchers, it is generally believed that this phenomenon only occurs during the mass/semi-mass flow discharge [4-5,37-38]. A common explanation of this phenomenon is the dynamic interaction between the silo side wall and the flowing bulk solids at the effective transition zone, i.e., the flow boundary between the upper plug and the bottom converging flows. This dynamic interaction leads to the variable friction between bulk solids and silo walls and thus induces the stick-slip motion of the granular assembly [4,5]. For funnel flow discharge, along the upward direction the flow zone width first increases and then keeps nearly constant, as shown in Fig.1 and Fig.2a. It is then natural to ask if the same mechanism can be applied for the resonance phenomenon observed in our simulation, i.e., the oscillatory motion of particles also emanates from the transition zone between the upper plug and the bottom converging flows. We will go back to this issue in next subsection.

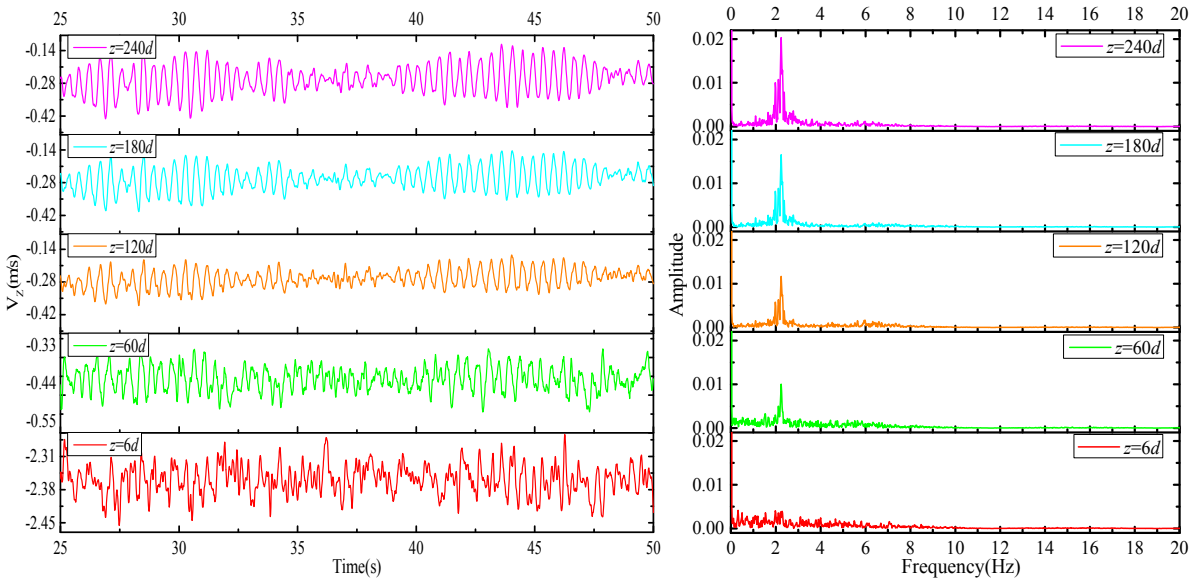

Fig.3 (a) The temporal variations of spatially averaged vertical velocity at different *z*-positions(*y*=0*d*), (b) the corresponding Fourier spectrums.

In order to quantify the time variation of particle vertical velocity, we calculated the root-mean-square (r.m.s.) vertical velocity fluctuation and the probability distribution function (PDF) of vertical velocity fluctuation. There could be three different ways to define the average velocity and thus the velocity fluctuation,

$$\overline{V}_j = \sum_{i=1}^{N_{P,j}} V_i / N_{P,j}, \quad \delta V_i = V_i - \overline{V}_j(t), \quad \overline{\Theta}_1 = \sum_{j=1}^{N_t} \sqrt{\sum_{i=1}^{N_{P,j}} \delta V_i^2 / N_{P,j}} / N_t \tag{4}$$

$$< \overline{V} >= \sum_{j=1}^{N_t} \overline{V}_j / N_t, \quad \delta V_j = \overline{V}_j - < \overline{V} >, \quad \overline{\Theta}_2 = \sqrt{\sum_{j=1}^{N_t} \delta V_j^2 / N_t}, \tag{5}$$

$$< V >= \sum_{j=1}^{N_t} \sum_{i=1}^{N_{P,j}} V_i / \sum_{j=1}^{N_t} N_{P,j}, \quad \delta V_i' = V_i - < V >, \quad \overline{\Theta}_3 = \sqrt{\sum_{j=1}^{N_t} \sum_{i=1}^{N_{P,j}} \delta V_i'^2 / \sum_{j=1}^{N_t} N_{P,j}} \tag{6}$$

Here, $N_{P,j}$ is the number of particles inside the considered statistical cell at the moment j, N_t

the total number of the sampling moment, V_i the vertical velocity of particle i. According to the definitions, $\overline{V}_j$ denotes the spatially averaged vertical velocity of particles in the statistical cell at the moment j, $<\overline{V}>$ is the time average result of $\overline{V}_j$, and $<V>$ is the average vertical velocity of all the particles appeared in the statistical cell in the whole sampling time interval. δV and $\overline{\Theta}$ represent the fluctuation of velocity and r.m.s. fluctuation velocity, respectively. δV_i reflects the random motion of particle i against the collective motion of particles in the considered region at given moment, and δV_j can be considered as the pseudo-turbulent fluctuation around the studied advective field [39]. When the statistical cell is too small to contain enough particles, Eq.6 is generally used to increase the number of sampling datum points [40,41]. Note that in our simulation particles move synchronously, as shown in Fig.2d and Fig.3a. Thus, results obtained from Eq.5 and 6 should be very close.

Fig.4a~c present the PDFs of the vertical velocity fluctuations defined in Eq. 4~6. The corresponding r.m.s. velocity fluctuations are shown in Fig.4d. It can be found from Fig.4a that the PDFs of the fluctuation of individual vertical velocity V_i around the instantaneous average $\overline{V}$ have fat tails compared to Gaussian distribution, suggesting the fluctuations of V_i around $\overline{V}$ are not stochastic. Fat-tailed PDFs of fluctuation velocity have been observed in

granular systems and attributed to the cage effect [42,43]: the random motion of particle relative to its neighbor particles in short time period is accompanied by the large and occasional jumps. This has been demonstrated by tracking the trajectory of particles: the random movement of particles is trapped in a finite volume before escaping and being trapped again in another finite volume [42,43]. Note that the shape of the fluctuation velocity PDF depends on how the velocity is calculated. When the velocity calculation is based on particle displacement and the time duration is long enough that the particle displacement is larger than the particle diameter, the PDF of fluctuation velocity will be Gaussian [43]. This phenomenon reflects that the motion of particles relative to its neighbor is super-diffusion in short time period but back to diffusion in longer time period [43,44]. Fig.4a shows that the PDF of V_i-$\overline{V}$is not symmetric about 0. This can be ascribed to the fact that gravity induces a preference for downwards movement. Fig.4a also indicate that the range of the fluctuation of V_i around $\overline{V}$ decrease sharply with the vertical position. This is further demonstrated in Fig.4d. It can be seen that for z >90d the r.m.s. fluctuation velocity $\overline{\Theta}_1$ is nearly zero.

Fig.4b presents the fluctuation of instantaneous average vertical velocity $\overline{V}$ around its long-time average <$\overline{V}$>. Different from the fluctuation of V_i-$\overline{V}$, the fluctuation of $\overline{V}$-<$\overline{V}$> is close to Gaussian. Such result suggests that the temporal fluctuation of $\overline{V}$ can be considered as a random process. Similar behavior has been found in both DEM simulations [45] and physical experiments [34]. It was reported that the auto-correlation of instantaneous average velocity $\overline{V}$ decreases to zero after the time that particle fall its own diameter [34,42]. Though data are

not presented here, our supplementary analyses show that this is also the case of our simulations. It can be seen from Fig.4d that the range of the fluctuation of $\overline{V}$ around $<\overline{V}>$, $\overline{\Theta}_2$, varies non-monotonously along the upward direction and displays a local minimum at $z \approx 90d$. We have carefully checked that decreasing the size of statistic cell to $1.5d$ does not influence such non-monotonous variation trend. As will be presented in next subsection, the resonant motion of particles appearing in the simulations originates from the mechanical fluctuation in a transition zone right above the outlet. For the case with $W_1=20d$, the position of this zone is around 40-$90d$. Starting from this transition zone and moving upward, the amplitude of vertical velocity fluctuation increases [7, 46], see also Fig.3a, leading to the increase of $\overline{\Theta}_2$.

Fig.4c presents the fluctuation of individual particle vertical velocity V around $<V>$, the average vertical velocity of all the particles appeared in the statistical cell in the whole sampling time interval. As to be expected, the PDFs of V-$<V>$ are similar to those of $\overline{V}$-$<\overline{V}>$ and close to Gaussian. Such results are in partially agreement with the experimental results reported by the group of Nott [40, 41]. They analyzed the PDFs of velocity fluctuation of particles next to the side wall through CCD imaging technology. Their experimental results show that for velocity smaller than $<V>$ the PDF is nearly Gaussian, whereas for velocity larger than $<V>$ it has a fat tail and decays as a power law when the fluctuation velocity is sufficiently large. They ascribed such asymmetrical distribution to the gravitational effect which induced the preference for downward velocity [40]. But they also admitted that this asymmetry could also be possibly due to the retarding effect of boundary wall [41]. Note that

Fig.4c is qualitatively consistent with the experimental results of Garcimartin et al[34]. These authors investigated the fluctuating movement of particles inside a discharging pseudo-2D silo. They found the PDFs of instantaneous average velocity ($\overline{V}$) around its long-time average $<\overline{V}>$ was nearly Gaussian. In their experiments, due to the collective and correlated motion of particles, the time variations of the velocity of individual particles (V) and instantaneous average velocity $\overline{V}$ were very close. It is thus reasonably to conjecture that the PDFs of V-$<V>$ will also be close to Gaussian.

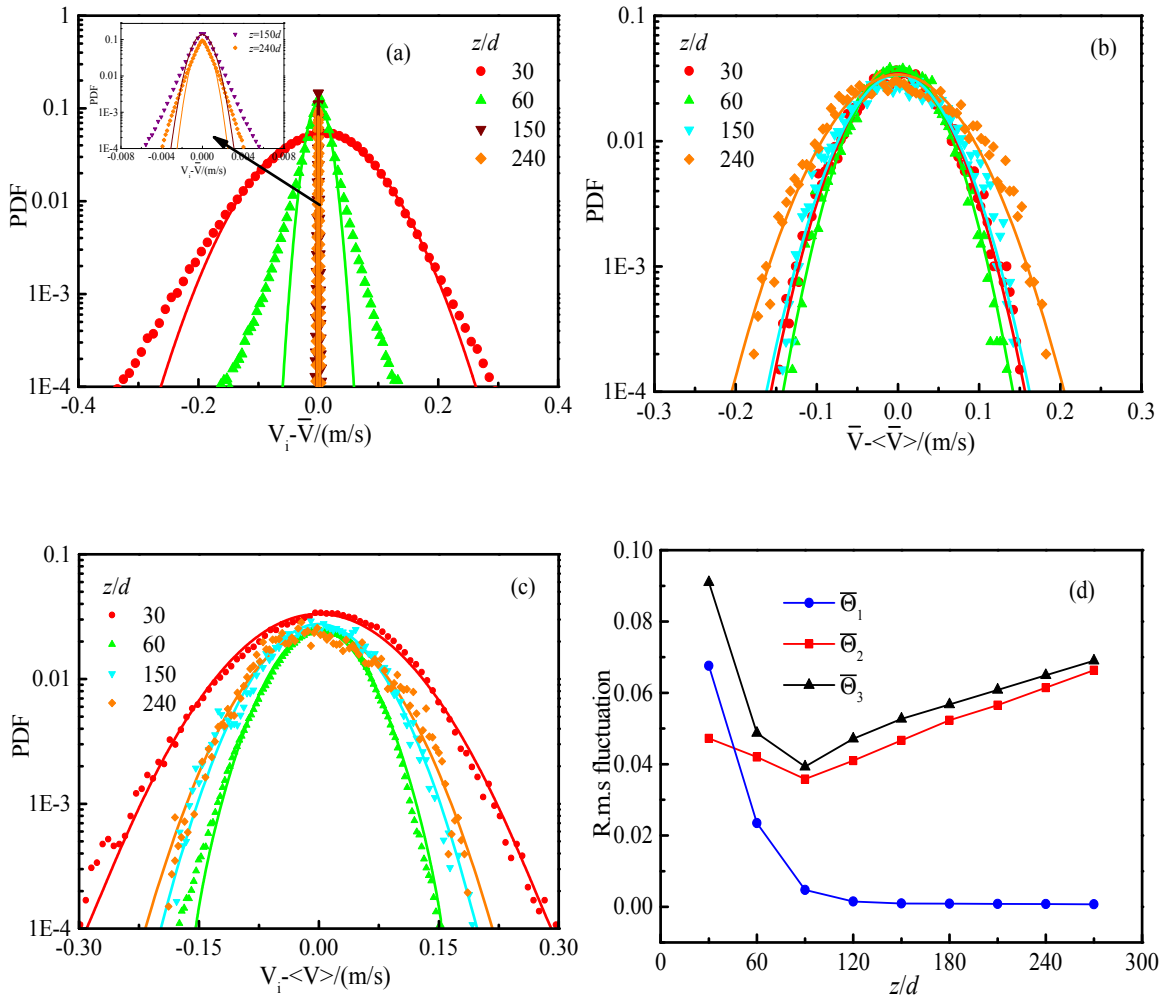

Fig.4 (a), (b) and (c) denotes the PDFs of δV_i, δV_j and $\delta V_i'$ at different z- positions(y=0d), respectively. The insert in Fig.4 (a) is the zooms of the PDFs at z=150d and z=240d

positions(y=0d). (d) The variations of r.m.s. vertical velocity fluctuations along vertical direction.

It is worth noting the clear difference between $\overline{\Theta}_1$ and $\overline{\Theta}_3$. It can be found from Fig.4d that by using different definitions of average velocity the obtained values of r.m.s. fluctuation velocity and also their spatial variation trends can be totally different. For z >90d, the shear rate at y=0 is negligibly small (Fig.2a). Thus, in this region the r.m.s. fluctuation velocity, which reflects the granular temperature, should be close to zero. Nevertheless, this is true only when the instantaneous spatial-averaged velocity $\overline{V}$ is adopted to calculate the r.m.s. fluctuation velocity. when <V> is used, the obtained r.m.s. fluctuation velocities in region with ignorable shear (z >90d) can be even larger than those in region with considerable shear (z <60d). This counterintuitive phenomenon in the discharge of particles from silo was first observed by Moka and Nott [40]. They attributed the abnormally large r.m.s. fluctuation velocity to the collective motion where particles interact through endured contact rather than instantaneous collision. Fig.4d indicates that r.m.s. fluctuation velocity is indeed ignorable in the plug flow zone once the collective motion is excluded. Such result also suggests that, in order to investigate the diffusive motion of individual particle in silo discharge, pseudo-turbulent fluctuation around the studied advective field (due to the gravity) should be excluded.

3.2 Correlation analyses

To identify the emission source of the above-mentioned resonant motion of particles, the delayed correlations between the time series of the fluctuation of $\overline{V}$ monitored at different z-

positions have been analyzed. This method has been adopted by different researchers to characterize the wave propagation during silo discharge [7-9]. For two time series data $X=\{x_1, \ldots, x_n\}$ and $Y=\{y_1,\ldots, y_n\}$, the correlation coefficient $C_{xy}(t)$ for a delayed time t (Y delay X) can be calculated as,

$$C_{xy}(t)=\frac{\sum_{\tau=t+1}^{n}(x_\tau-\bar{x})(y_{\tau-t}-\bar{y})}{\sqrt{\sum_{\tau=t+1}^{n}(x_\tau-\bar{x})^2}\sqrt{\sum_{\tau=1}^{n-t}(y_\tau-\bar{y})^2}}$$

$$\bar{x}=\frac{1}{n-t}\sum_{\tau=t+1}^{n}x_\tau,\quad \bar{y}=\frac{1}{n-t}\sum_{\tau=1}^{n-\tau}y_\tau \qquad (7)$$

where the maximum value of t is $n/2$ and n denotes the total number of datum points. The time when C_{xy} achieves its maximum is the delayed time of Y relative to X . The magnitude of $C_{xy}(t)$ is obviously dependent on the fluctuation of the data ($x_\tau-\bar{x}$, $y_\tau-\bar{y}$). Thus, in our analyses the fluctuations of $\overline{V}$ around the average $<\overline{V}>$ were all normalized by the r.m.s. fluctuation velocity $((\overline{V}-¿\overline{V}>¿)/\overline{\Theta}_2)$.

Fig.5a shows the delayed correlations between the normalized fluctuation velocity at the reference height z=270d (y=0) and those at lower vertical positions (y=0). It can be found that the fluctuations of particle velocity at different vertical positions are strongly correlated. The insert figure shown in Fig.5a is the delay correlation of the normalized velocity fluctuation at the height z=18d (y=0). Although the Fourier spectrum at z=18d do not present distinguishable structure (Fig.3b), the maximum correlation coefficient between the fluctuations of velocity at z=270d and z=18d is as large as 0.42. A close check of the Fourier spectrum at z=18d indicates that, being consistent with the location of the predominant peak

of the Fourier spectrum at z=270d, there do exist a peak at the frequency of around 2.24Hz. Such results suggest there exist a unique emission source responsible for the fluctuation of particle velocity, though the regularity of particle velocity fluctuation in region close to outlet is blurred by random noise.

In Fig.5a the time corresponding to the maximum of C_{xy} denotes the delayed time of the fluctuation velocity at z=270d relative to that at other vertical position (The time signal of the fluctuation velocity at z=270d was treated as Y in Eq.7). Fig.5b presents the vertical variation of the delayed time. Along the downward direction, the delayed time first slightly increases, then sharply increases before decreasing again. A turning point appears at the vertical position $z \approx 42d$.. According to the definitions of delayed correlation, the slight decrease of the delayed time suggests the formation of resonant motion of particles in the upper part of the flowing zone, and the appearance of the turning point indicates the location of the emission source of the fluctuation [7]: fluctuation first appears at the turning point and it propagates both upward and downward.

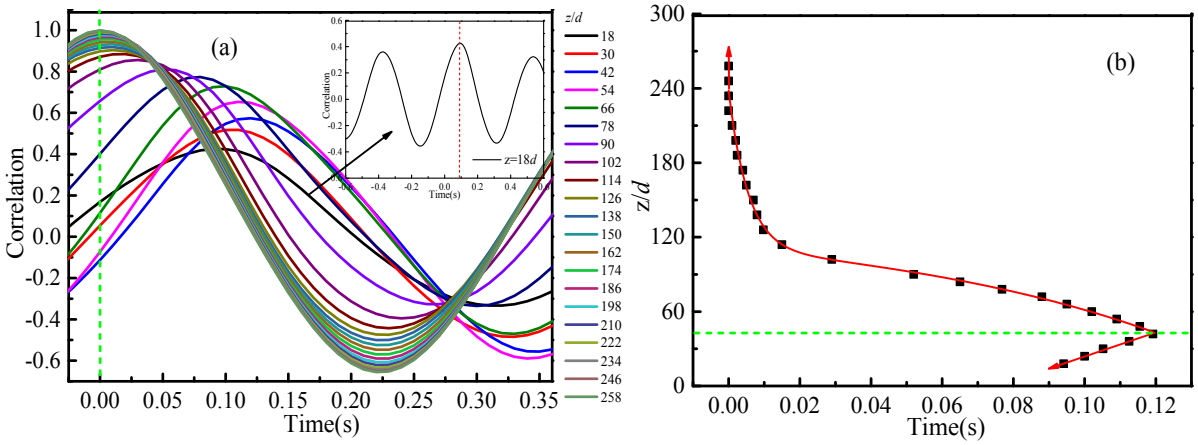

Fig.5 (a) The delayed correlations between the normalized fluctuation velocity at the

reference height z=270d (y=0) and those at lower vertical positions (y=0), the insert is the delayed correlation between the velocity fluctuations at z=18d and z=270d (y=0). (b) The vertical variation of the delayed time.

The regular fluctuation of particle vertical velocity during the silo discharge is generally attributed to the fluctuation of interaction forces between particles [7-9]. As to the platform of EDEM2.7, the contact information is represented by the parameter of compressive force which is the sum of the surface normal force magnitudes. Fig.6a presents the Fourier spectrum of the time-signals of the spatially averaged compressive force $\overline{F}$ as a function of vertical position. For comparison reason, Fig.6b presents the Fourier spectrum of the time-signals of the spatially averaged vertical velocity $\overline{V}$. It can be found that these two spectrums share similar patterns and both have a predominant peak at the frequency of 2.24Hz. As to be expected, the vertical variation of the frequency peak for $\overline{V}$is similar to that of $\overline{\Theta}_2$ (see Fig.4d). The variation of the magnitude of frequency peak for $\overline{F}$ along the vertical direction is also non-monotonous. The predominant peak first appears at z ≈42d, which coincides with the position of turning point in the delayed time profile (Fig.5b). Starting from this position and moving upward, the magnitude of frequency peak for $\overline{F}$ first increases and then decreases. The location of the turning points is around z=90d. Again, this position coincides with the location of a minimum value of the magnitude of frequency peak for $\overline{V}$ (and also $\overline{\Theta}_2$, see Fig.4d).

Fig.6c presents the correlation coefficient between the dimensionless fluctuations of $\overline{F}$ and $\overline{V}$

(normalized by their r.m.s. fluctuation values) as a function of the delayed time of the latter for an observation window at z=180d. The graph clearly indicates that these two variables are strongly correlated but not synchronized, as the maximal correlation does not locate at t=0. Note that in our calculations $\overline{V}$ is negative and $\overline{F}$ is positive. Thus, Fig.6c indicates that the occurrence of the minimum vertical velocity magnitude is preceded by the maximal compressive force, vice versa. Note that, being consistent with the characteristic frequencies of the fluctuations of these two variables, the time interval between the neighboring minimal and maximal values of correlation coefficient is around 0.22s ($\approx\frac{0.5}{2.24\,\mathrm{Hz}}$) . The delayed correlation between $\overline{F}$ and $\overline{V}$ thus supports the hypothesis that the velocity fluctuation of particles during silo discharge is originated from the dynamic variations of the mechanical interactions between particles [7-9], as mentioned in the introduction section.

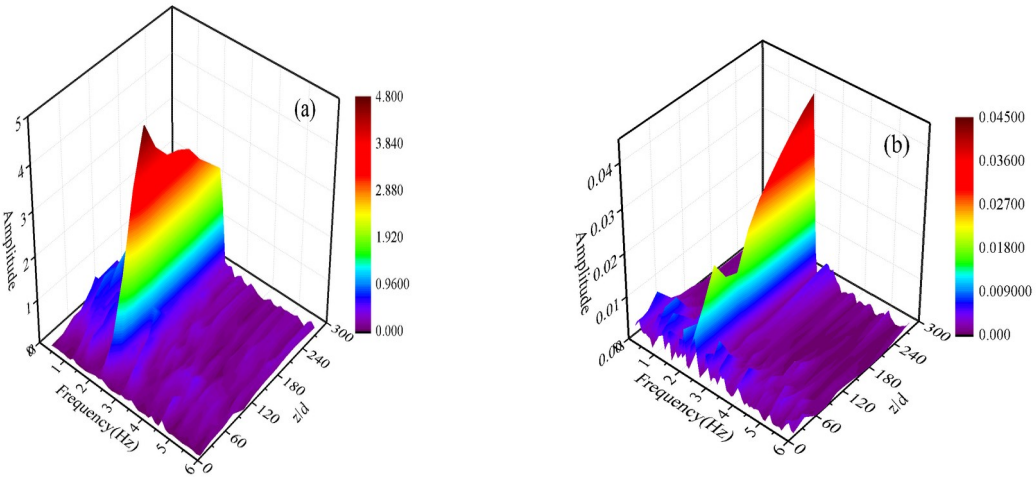

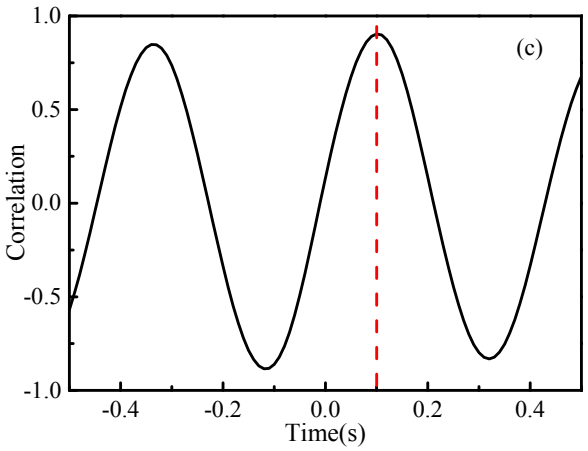

Fig.6 Fourier spectrums of the time-signals of the spatially averaged compressive force (a) and vertical velocity (b). (c) The correlation between the normalized fluctuations of compressive force and vertical velocity as a function of the delayed time for an observation window at z= 180d.

3.3 Discussions

Based on the above analyses, it can be found that in the simulated silo there are two special vertical positions. The lower one corresponds to the turning point in the delayed time profile (Fig.5b), and the upper one corresponds to the location of local minimum (maximum) in $\overline{\Theta}_2$ (fluctuation amplitude of $\overline{F}$) profile. Fig.2b and Fig.7 summarizes the simulation results for different outlet sizes. The possible effect of frictional coefficient has also been evaluated. Within the considered range (μ =0.2~0.8), frictional coefficient affects the fluctuation amplitudes of the considered parameters, but its influence on the locations of the two special vertical positions are nearly ignorable.

Fig.2b and Fig.7a~c suggests that the appearances of the two special vertical positions seem

to be robust. We start with the upper one. It can be seen from Fig.2b and Fig.7a~b that there exists turning point in the profiles of <V>, $\overline{\Theta}_2$ and A_{Fc} (fluctuation amplitude of $\overline{F}$). The absolute value of <V> first decreases with the vertical position and then flattens out (Fig.2b). As discussed in section 3.1, constant <V> reflects the formation of plug flow. It can be seen from Fig.2 that the width of flowing zone is nearly constant in the plug flow region. Thus, the turning point in the profile of <V> actually designates the converging of the flowing zone. Its location is approximately at z=60d, 90d, 120d, 138d for W_1=10d, 20d, 30d, 40d, respectively. The locations of the turning points in the $\overline{\Theta}_2$ profiles are around at 60d, 90d, 120d, 120d, and those in the A_{Fc} profiles 66d, 102d, 126d, 150d. It can be found that for given W_1 the locations of the three turning points are close to each other. Qualitatively, this phenomenon is similar to that appears in the mass/semi-mass flow silos. It has been well recognized that in mass/semi-mass flow silos the most violent fluctuation of wall normal pressure appears at the Effective Transition Point (ETP) at which the flowing zone starts to converge downwardly [4,6,11-13]. The severe pressure fluctuation is generally attributed to the direction change of the major principal stress of the bulk material: the direction of the major principal stress turns from vertical (above EPT) to horizontal (below EPT), leading to the formation of shear zones in the converging part [6]. The significant pressure fluctuation at EPT can cause the formation of stick-slip behavior between bulk material and the silo wall. And such stick-slip mechanism has been suggested to be the source of resonance (honking/quaking) observed in mass/semi-mass flow silos [4,6]. Nevertheless, there are also experimental evidences that resonance can appear in silos with very rough walls where stick-slip motion of bulk material relative to the silo wall could not occur [4]. The occurrence of resonance in our funnel flow silo also hints

that the stick-slip behavior is not a necessary condition. As mentioned previously, resonance has also been observed in fully three-dimensional funnel flow silo with wedged-shaped bottom. In that case, the resonant motion of particles is ascribed to the instability of stagnant zone: the occasional slipping of the material from a stagnant zone leads to the formation of mechanical shock [6]. We have carefully checked that in the flat-bottomed silos considered here the stagnant zones are quite stable and did not observe any slipping event. The persistent regular fluctuation of particle velocity shown in Fig.4 also firmly rejects the occasionally slipping mechanism.

Fig.7c indicates that in our simulations the resonant motion of particles in the plug flow region emanates from the converging zone. The locations of the emanation source are around at z=30d, 42d, 66d, 90d for W_1=10d, 20d, 30d, 40d, respectively. A possible explanation of this emanation source is the formation of free-fall arch. The free-fall arch idea has been referred frequently by different researchers to understand the widely accepted formula of flow rates called “Beverloo laws” [47-50]. According to this assumption, particles are subjected to contacting stress above the arch and move downward freely due to gravity below the arch, i.e., the stress in the flow direction vanishes at the location of arch. Experimental and numerical evidences supporting this hypothesis have been reported in literature. Vivanco et al. [9] onducted experiments on the flow of photoelastic disks in a two-dimensional wedged-shaped silo and detected the formation of intermittent force chain network right above and close to the outlet. They found that the buildup and failure of the force chain network led to notable fluctuation of particle velocity. Mollon and Zhao [7] investigated the

local fluctuations during a 2D wedged-shaped hopper granular flow. Resonant motion of particles with characteristic frequency also appeared in their DEM simulations. Their analyses also showed that the oscillatory fluctuation of particle velocity magnitude originated from the lower center of the hopper where periodic buildup and failure of force chain networks occurred. Due to the dynamic characteristics of force chains, and also the fact that the fluctuation is more likely originated from the collective behavior of force chains (i.e., force chain network), precisely quantifying the location of the free-fall arch is difficult, especially for three-dimensional silo [49]. Free-fall arch with vertical location ranging from half to several outlet sizes have been suggested by different researchers [7,9,47-50]. Note that in our simulations the vertical location of the emanation source is around $2W_1$, which is consistent with the findings of Mollon and Zhao [7] and Lin et al [50]. In the DEM simulations of Mollon and Zhao [7] the emission source located at around 1.4 times outlet size. Lin et al [50] investigated the influence of outlet size on the vertical location of free-fall arch through 2D DEM simulations and found that the latter was about 2~3 times outlet size.

We found that the appearance of the above mentioned two special vertical positions can also be captured through the vertical profile of solid volume fraction at y=0, as shown in Fig.7d. The presented results were directly exported from the EDEM software. Note that EDEM uses an approximate way to calculate the solid volume fraction: particle is considered as being fully inside a statistical cell once its centroid is in that cell. Thus, the results presented in Fig.7d is only qualitative. For all the considered outlet sizes, solid volume fraction first slightly rises and then sharply increases to a nearly constant value. The vertical positions of

the two turning points coincides very well with those of the bottom emission source and the upper converging point of flowing zone. Qualitatively, the variation trend of solid volume fraction shown in Fig.7d is in good agreement with DEM results of Drozd and Denniston [51]. Based on particle velocity, these authors distinguished granular flow in silo into three regions: free fall, fluid and glassy regions, from bottom to top, respectively. They found that solid volume fraction sharply increased in the intermediate fluid region, whereas in other two regions it nearly kept constant. Similar findings have also been reported by Vidyapati and Subramaniam [52], though these authors used different names (inertial, intermediate and quasi-static regions) and definition standard (mean strain rate). Their DEM results also indicate that the most violent fluctuation of particle stress appears in the upper part of intermediate region.

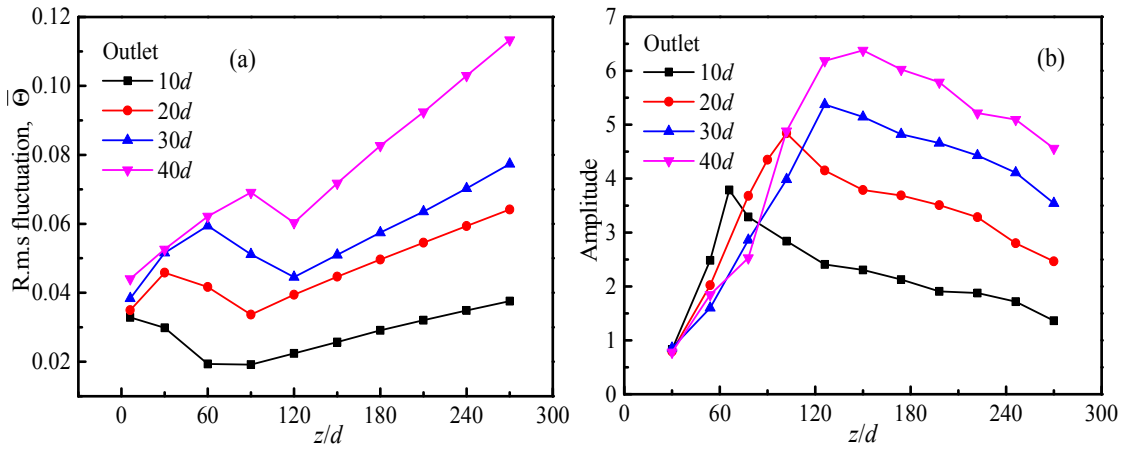

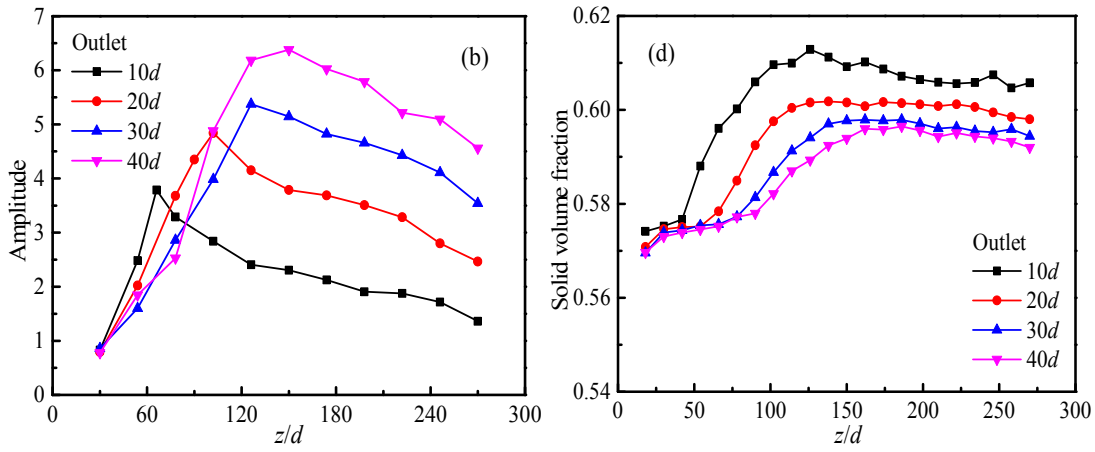

Fig.7 Vertical profiles of r.m.s fluctuation of spatially averaged vertical velocity (a), fluctuation amplitude of compressive force(b), delayed time (c) and solid volume fraction (d).

In brief, Fig.2b and Fig.7 indicates that at the bottom part of the funnel flow silo there exists an intermediate/fluid region. At its lower boundary particle contact force fluctuates with a predominant frequency, which subsequently leads to the oscillatory variations of particle velocity. Its upper boundary corresponds to the transition position from which the flowing zone width starts to keep nearly constant. Similar to mass/semi-mass flow silo, at this upper boundary the fluctuation of particle contact force is the most violent. The DEM and continuum simulation results of Vidyapati and Subramaniam [52] suggest that this intermediate region plays a key role in the discharge dynamics of silo. Experimental evidences demonstrating the importance of this intermediate region have also been reported in literature. It has been found that the clogging of granular flow in silo can be significantly reduced or even suppressed by putting an obstacle at 1~2 times outlet size above the outlet [53,54]. For stable silo discharge installing an obstacle at a proper position of the bottom converging zone can even lead to higher flow rate than the case without obstacle [14,18-20].

Based on the simulation results presented here, it can be reasonably deduced that the presence of obstacle can modify the fluctuating characteristics of flow field. We thus infer that this might be one of the reasons for the increase of flow rate. We will test this conjecture in our future work.

4. Conclusions

Strong fluctuations in velocity and stress fields have been frequently observed in mass/semi-mass flow silos. Though it is reported that such phenomena can also appear in funnel flow silos, the considered silos are generally either pseudo-2D or wedge-shaped. The primary motivation of this study is to explore whether the commonly proposed mechanisms of fluctuations in mass/semi-mass flow silos also apply for funnel flow silo. The discharges of granular particles from funnel flow silos were then investigated through 3D DEM simulations. The simulated silos have flat-bottomed structure to avoid the occasional slipping of stagnant zone material. Periodic boundary conditions were adopted in the depth direction to exclude the possible front and rear wall effects. Our simulation results demonstrate that in the main part of the flowing zone particle vertical velocity fluctuates with a characteristic frequency, suggesting the formation of resonance. Parameter analyses were conducted to understand the formation of such flow fluctuation, including the delayed correlations of velocity fluctuations at different vertical positions, the Fourier spectrums of vertical velocity and contact force, axial profiles of r.m.s. vertical velocity fluctuations and solid volume fraction. Within the considered outlet size range, we found that there always exist two special vertical positions in the converging part of the flowing zone. Regular fluctuations of vertical

velocity emanate from the lower position and propagate both upwards and downwards. The higher position locates at the upper boundary of converging part of the flowing zone and is characterized by the most violent fluctuation of contact force. Our simulation results thus suggest that there is no intrinsic difference between the oscillatory fluctuations appeared in funnel flow silo and those in mass/semi-mass flow silo. Our simulations also indicate that stick-slip motion between bulk materials and silo wall is not a necessary condition for the occurrence of resonance.

Acknowledgments

The authors acknowledge financial supports from The National Key Research and Development Program of China, Grant No. 2016YFF0102601, Innovation Academy for Green Manufacture, Chinese Academy of Sciences (IAGM-2019-A13)

References

1. Saleh K, Golshan S, Zarghami R. A review on gravity flow of free-flowing granular solids in silos-Basics and practical aspects. Chemical Engineering Science. 2018;192:1011-1035.

2. GDR MiDi. On dense granular flows. The European Physical Journal E. 2004;14: 341-365.
3. Forterre Y, Pouliquen O. Flows of Dense granular media. Annual Review of Fluid Mechanics. 2008;40:1-24.
4. Wilde K, Tejchman J. Silo music–Mechanism of dynamic flow and structure interaction. Powder Technology. 2008;186:113-129.
5. Wilde K, Tejchman, J, Rucka M, Niedostatkiewicz M. Experimental and theoretical investigations of silo music. Powder Technology. 2010;198: 38-48.
6. Schulze D. Powders and Bulk solids: Behavior, Characterization, Storage and Flow, Springer Berlin Heidelberg, 2008.
7. Mollon G, Zhao J. Characterization of fluctuations in granular hopper flow. Granular Matter. 2013;15: 827-840.
8. Gardel E, Seitaridou E, Facto K, Keene E, Hattam K, Easwar N, Menon N. Dynamical fluctuations in dense granular flows. Philosophical Transactions. 2009;367: 5109-5121.
9. Vivanco F, Rica S, Melo F. Dynamical arching in a two dimensional granular flow. Granular Matter. 2012;14, 563-576.
10. Buick JM, Pankaj, Ooi JY, Chavez-Sagarnaga J, Pearce A, Houghton G. Motion of granular particles on the wall of a model silo and the associated wall vibrations. Journal of Physics D: Applied Physics. 2004;37: 2751-2760.
11. Ostendorf M, Schwedes J. Application of particle image velocimetry for velocity measurements during silo discharge. Powder Technology. 2005;158: 69-75.
12. Wang Y, Lu Y, Ooi JY. Finite element modelling of wall pressures in a cylindrical silo with conical hopper using an arbitrary Lagrangian-Eulerian formulation. Powder

Technology. 2014;257: 181-190.

13. Wang X, Liang C, Guo X, Chen Y, Liu D, Ma J, Chen X, An H. Experimental study on the dynamic characteristics of wall normal stresses during silo discharge. Powder Technology. 2020;363: 509-518.
14. Baxter GW, Behringer RP. Pattern formation in flowing sand. Physical Review Letters. 1989;62: 2825-2828.
15. Le Pennec T, Ammi M, Messager JC, Valance A. Dynamics of density waves in a two dimensional funnel on an inclined plane. The European Physical Journal B. 1999;7: 657-664.
16. Fullard LA, Davies CE, Lube G, Neather AC, Breard ECP, Shepherd BJ. The transient dynamics of dilation waves in granular phase transitions during silo discharge. Granular Matter. 2017;19:6.
17. Roberts AW, Wensrich CM. flow dynamics or ‘quaking’ in gravity discharge from silos. Chemical Engineering Science. 2002;57: 295-305.
18. Katsuragi H, Reddy KA, Endo K. Shape dependence of resistance force exerted on an obstacle placed in a gravity-driven granular silo flow. AICHE Journal. 2018;64: 3849-3856.
19. Alonso-Marroquin F, Azeezullah SI, Galindo-Torres SA, Olsen-Kettle LM. Bottlenecks in granular flow: When does an obstacle increase the flow rate in an hourglass. Physical Review E. 2012;85: 020301.
20. Hsiau SS, Smid J, Chyou YP, Liu TC, Huang TC, Hsu CJ. Impact of flow-corrective insert on flow patterns in two-dimensional moving bed. Chemical Engineering and

Processing: Process Intensification. 2013;73: 7-15.

21. Tian T, Su JL, Zhan JH, Geng SJ, Liu XX. Discrete and continuum modeling of granular flow in silo discharge. Particuology. 2018;36, 127-138.
22. Drescher A, Ferjani M. Revised model for plug/funnel flow in bins. Powder Technology. 2004;141, 44–54.
23. Babout L, Grudzien K, Maire E, Withers PJ. Influence of wall roughness and packing density on stagnant zone formation during funnel flow discharge from a silo: An X-ray imaging study. Chemical Engineering Science. 2013;97, 210–224.
24. Maiti R, Das G, Das PK. Experiments on eccentric granular discharge from a quasi-two-dimensional silo. Powder Technology. 2016;201: 1054-1066.
25. Maiti R, Meena S, Das PK, Das G. Flow field during eccentric discharge from quasi-two-dimensional silos-extension of the kinematic model with validation. AIChE Journal. 2016;62: 1439-1453.
26. Sielamowicz I, Blonski S, Kowalewski TA. Optical technique DPIV in measurements of granular material flows, Part 1 of 3—plane hoppers. Chemical Engineering Science. 2005;60: 589-598.
27. Lattanzi AM, Stickel JJ. Hopper flows of mixtures of spherical and rod-like particles via the multisphere method. AIChE Journal. 2020;66(4):16882.
28. Szabo B, Kovacs Z, Wegner S, Ashour A, Fischer D, Stannarius R, Borzsonyi T. Flow of anisometric particles in a quasi-two-dimensional hopper. Physical Review E. 2018;97: 062904.
29. Zhou YC, Wright BD, Yang RY, Xu BH, Yu AB. Rolling friction in the dynamic simulation of sandpile formation. Physica A. 1999;269: 536-553.

30. Zhu HP, Yu AB. The effects of wall and rolling resistance on the couple stress of granular materials in vertical flow. Physica A. 2003;325: 347-360.
31. Iwashita K, Oda M. Rolling resistance at contacts in simulation of shear band development by DEM. Journal of Engineering Mechanics. 1998;124: 285-292.
32. Ketterhagen WR, Curtis JS, Wassgren CR, Hancock BC. Predicting the flow mode from hoppers using the discrete element method. Powder Technology. 2009;195:1-10.
33. Xiao X, Su JL, Xu G, Cui L, Liu XX. Discrete modeling of discharge dynamics of granular material in moving bed: effect of outlet setting. CIESC Journal. 2016;67: 1710-1718.
34. Garcimartin A, Zuriguel I, Janda A, Maza D. Fluctuations of grains inside a discharging two-dimensional silo. Physical Review E. 2011; 84: 031309.
35. Zuriguel I, Maza D, Janda A, Hidalgo RC, Garcimartin A. Velocity fluctuations inside two and three dimensional silos. Granular Matter. 2019;21:47.
36. Cleary PW, Sawley ML. DEM modelling of industrial granular flows: 3D case studies and the effect of particle shape on hopper discharge. Applied Mathematical Modelling. 2002;26: 89-111.
37. Borzsonyi T, Kovacs Z. High-speed imaging of traveling waves in a granular material during silo discharge. Physical Review E. 2011;2011: 032301.
38. Babout L, Grudzien K, Maire E, Withers PJ. Influence of wall roughness and packing density on stagnant zone formation during funnel flow discharge from a silo: An X-ray imaging study. Chemical Engineering Science. 2013;97: 210-224.
39. Jung J, Gidaspow D. Measurement of two kinds of granular temperatures, stresses and dispersion in bubbling beds. Industrial & Engineering chemistry Research. 2005;44:

1329-1341.

40. Moka S, Nott PR. Statistics of particle velocities in dense granular flows. Physical Review Letters. 2005;95: 068003.
41. Ananda KS, Moka S, Nott PR. Kinematics and statistics of dense, slow granular flow through vertical channels. Journal of Fluid Mechanics. 2008;610: 69-97.
42. Pouliquen O, Belzons M, Nicolas M. Fluctuating particle motion during shear induced granular compaction. Physical Review Letters. 2003;91: 014301.
43. Choi J, Kudrolli A, Rosales RR, Bazant MZ. Diffusion and mixing in gravity-driven dense granular flows. Physical Review Letters. 2004;92: 174301.
44. Kharel P, Rognon P. Shear-induced diffusion in non-local granular flows. EPL. 2018;124: 24002.
45. Tewari S, Tithi b, Ferguson A, Chakraborty B. Growing length scale in gravity-driven dense granular flow. Physical Review E. 2009;79: 011303.
46. Borzsonyi T, Kovacs Z. High-speed imaging of traveling waves in a granular material during silo discharge. Physical Review E. 2011;83: 032301.
47. Hilton JE, Cleary PW. Granular flow during hopper discharge. Physical Review E. 2011;84: 011307.
48. Oldal I, Keppler I, Csizmadia B, Fenyvesi L. Outflow properties of silos: the effect of arching. Advanced Powder Technology. 2012;23: 290-297.
49. Rubio-Largo SM, Janda A, Maza D, Zuriguel I, Hidalgo RC. Disentangling the free-fall arch paradox in silo discharge. Physical Review Letters. 2015;114: 238002.
50. Lin P, Zhang S, Qi J, Xing YM, Yang L. Numerical study of free-fall arches in hopper flow. Physica A. 2015;417: 29-40.

51. Drozd JJ, Colin D. Velocity fluctuations in dense granular flow. Physical Review E.2008;78: 041304.
52. Vidyapati V, Subramaniam S. Granular flow in silo discharge: Discrete element method simulations and model assessment. Industrial & Engineering Chemistry Research. 2013;36: 13171-13182.
53. Zuriguel I, Janda A, Garcimartin A, Lozano C, Arevalo R, Maza D. Silo clogging reduction by the presence of an obstacle. Physical Review Letters. 2011;107: 278001.
54. Endo K, Reddy KA, Katsuragi H. Obstacle-shape effect in a two-dimensional granular silo flow field. Physical Review Fluids. 2017;2: 094302.